Tracer Kinetic Modeling Approaches for the Quantification of Hepatic Function with Technetium-99m DISIDA and Scintigraphy

Sanjiv S. Gambhir, Randall A. Hawkins, Sung-Cheng Huang, Theodore R. Hall, Ronald W. Busuttil, and Michael E. Phelps

Division of Nuclear Medicine and Biophysics, Department of Radiological Sciences, Department of Surgery, and Laboratory of Nuclear Medicine, UCLA School of Medicine, Los Angeles, California

Serial scintigraphic images following injection of [^{99m}Tc]iminodiacetic acid compounds such as [^{99m}Tc]diisopropyl-iminodiacetic acid (DISIDA) provide qualitative information about liver function. We have investigated approaches for quantitatively describing liver function in terms of the kinetics of DISIDA extraction and excretion by the liver. Several compartmental model configurations were evaluated. A three-compartment model (blood, hepatic parenchyma, intrahepatic bile) was found to fit the data best and was used in conjunction with dynamic image data to obtain estimates of rate constants for liver extraction and excretion of DISIDA, and mean residence time (MRT) of DISIDA in the liver. A noncompartmental approach based on a parametric deconvolution technique was also used to estimate the noncompartmental mean residence time (MRT^{nc}). To assess limitations of the noncompartmental approach, computer simulations were performed using the three-compartment model to generate time-activity curves followed by analysis of these curves by the noncompartmental method. The effect of plasma total bilirubin level on DISIDA uptake and MRT was also investigated. These techniques are readily adaptable to standard nuclear medicine computing facilities, and could be used in the clinical setting to numerically describe serial DISIDA studies (especially in liver transplant patients) efficiently and noninvasively.

J Nucl Med 30:1507–1518, 1989

Assessment of the patency of the common bile duct and cystic duct are well-established indications for examination of the liver with technetium-99m (^{99m}Tc) iminodiacetic acid (HIDA) compounds. Because HIDA compounds are extracted by the hepatocyte and excreted unconjugated into the bile, dynamic studies with HIDA are becoming increasingly useful for evaluation of the functional status of the liver, particularly with liver transplants (*1*). While functional changes in the liver will produce alterations in hepatocyte extraction and excretion of HIDA, most clinical applications of the technique have been based upon qualitative descriptions of HIDA dynamics. Several investigators have applied various types of quantitative analysis to dynamic HIDA studies in an attempt to generate a more objective characterization of changes in liver function with HIDA. Attempts at quantitation include measurements of the time of peak activity in the liver (t_{max}) and the time for half of this activity to clear from the liver ($t_{\frac{1}{2}}$) (*2–4*), and indices of extraction from plasma to hepatocyte (*5*). Deconvolution approaches for obtaining mean transit time of various tracers through the liver (as well as other organs) have also been studied (*6–12*).

We have employed compartmental modeling techniques with dynamic HIDA data to investigate several quantitative parameters of potential clinical usefulness, including rate constants for transport (from plasma) and excretion (from liver) and the mean residence time (MRT) of HIDA in the liver. We have also employed a noncompartmental method based on parametric de-

Received Oct. 19, 1988; revision accepted June 7, 1989.

For reprints contact: R.A. Hawkins, MD, PhD, Div. of Nuclear Medicine and Biophysics, Dept. of Radiological Sciences, UCLA School of Medicine, Los Angeles, CA 90024.

convolution to estimate the noncompartmental mean residence time (MRT^{nc}). Although absolute quantitation from gamma camera scans is inherently limited because of the lack of accurate attenuation correction and crossover of activity (i.e., precise measurements of activity concentrations in tissue are not possible even with single photon emission computed tomography (SPECT) data, and planar images clearly produce time-activity measurements affected by a variety of physical and anatomic factors), quantitation within these limitations should allow for the assessment of model parameters and for following directional changes in parameters in serial studies.

Although various radiopharmaceuticals have been used as tracers for imaging hepatobiliary disorders, HIDA compounds are the most widespread in use. These agents have relatively short hepatic transit times for analysis during a 1 hr study interval, are rapidly excreted into the bile, and thus provide ideal images with high contrast between the liver and the intrahepatic bile ducts. Diisopropyl-iminodiacetic acid (DISIDA, diisopropyl IDA) is the most commonly used IDA compound because it has a high liver to renal extraction, and its uptake by the liver is not as highly dependent on serum bilirubin levels (a competitive inhibitor for liver uptake) as are other tracers from the IDA family (*13–15*).

In order to model mathematically the uptake and excretion of DISIDA by the liver, it is important to understand the underlying physiologic and biochemical processes that govern these processes. Radioactive tracer is delivered to the sinusoids of the liver via both the portal vein and the hepatic artery. From the sinusoids the tracer diffuses through the pores in the endothelial lining to bind to a specific membrane bound carrier, which transports the tracer across the hepatocyte membrane and into the hepatocyte (*16*). Once inside the hepatocyte, the tracer may be bound by various enzymes and/or undergo metabolism. The excretion of tracer into intrahepatic bile ducts is thought to occur via active transport. From the intrahepatic bile ducts tracer is taken to the extrahepatic bile via choleresis. From here it may enter the duodenum directly or be stored in the gallbladder for later release. Once inside the intestines, DISIDA does not enter the enterohepatic circulation and is thus effectively removed from the system of interest. Although liver uptake and excretion of hepatobiliary agents follow nonlinear Michaelis-Menten kinetics, for tracer studies the exchange between compartments can be assumed to be first order as long as the tracer itself does not cause a significant degree of saturation of carriers and/or storage sites. In liver function studies only trace amounts of DISIDA (insufficient to saturate the system) are being used. Bilirubin competes with DISIDA for carrier transport sites, and the use of serum bilirubin levels in conjunction with quantitative estimates of liver uptake and excretion may be necessary to properly assess hepatic function (*13–15*).

An in vivo pharmacokinetic model based on a simplification of the above mechanisms is illustrated in Figure 1 (based on the model suggested in Reference *16*). As this model depicts, tracer is exchangeable between the vascular and extravascular space and the liver, as well as between the vascular and extravascular space and kidneys. From the liver the tracer may return to the blood pool or be transferred to the bile compartment. Once inside the bile compartment the tracer can only undergo excretion out of the system. From the kidney the tracer can only be excreted. Underlying this compartmental model configuration are several assumptions. It is assumed that blood flow to the liver does not limit the extraction of tracer from the blood. Second, each compartment is assumed to act in a kinetically distinct and homogeneous manner. Treatment of a given organ or tissue type as a single compartment is an approximation commonly employed in compartmental modeling. Transfer between compartments is assumed to be first order (i.e., the rate constants representing the fraction of tracer transferred from one compartment to another per unit time are in units of

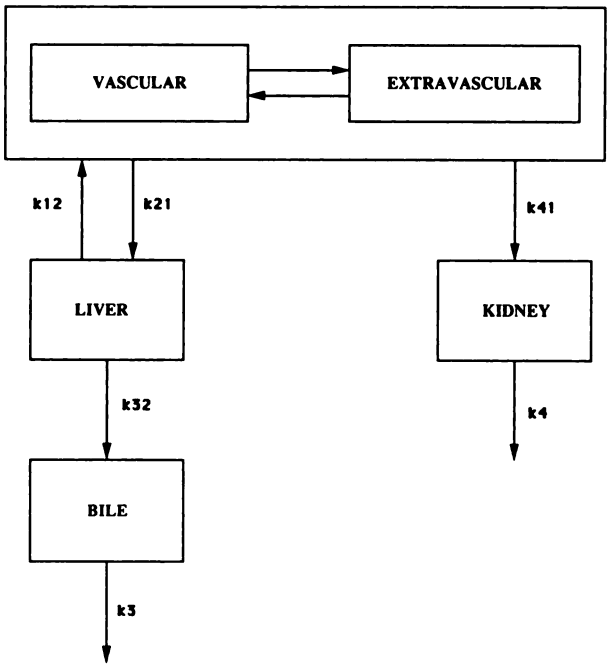

FIGURE 1
An in vivo pharmacokinetic model for HIDA. The blood pool is represented by an extravascular and vascular compartment. Exchange is possible with these and the liver compartment (as governed by rate constants k_{12} and k_{21}), and with the kidney compartment (as governed by k_{41}). Tracer from the liver is excreted to the bile compartment as governed by k_{32}, and from bile to the G.I. tract as governed by k_3. Tracer may also exit the kidneys out into urine as governed by k_4.

reciprocal time). In this model the liver is modeled as a single compartment representing hepatocytes, vasculature, as well as intrahepatic bile ducts.

A noncompartmental model can also be used to evaluate HIDA kinetics. A noncompartmental model is shown in Figure 2. The mathematic integral equations from this model can be used to estimate MRT^{nc}. A noncompartmental model is equivalent to any multicompartmental model when all inputs, leaks, and measurements are from the same central (liver) pool. In this case $MRT = MRT^{nc}$ (*17*).

METHODS

Scintigraphic Technique

Studies were performed using a bolus injection of 5 mCi [^{99m}Tc]DISIDA in adults, and proportionately less in children, followed by sequential imaging in an anterior position over the abdomen and lower thorax for a period of 1 hr. The studies were acquired with a 64 × 64 matrix using a large field of view gamma camera interfaced to a computer and display system, permitting region of interest definition over the imaged portion of the heart and liver. The imaging protocol consisted of 30 images, each of duration 2 min, for a total acquisition time of 1 hr.

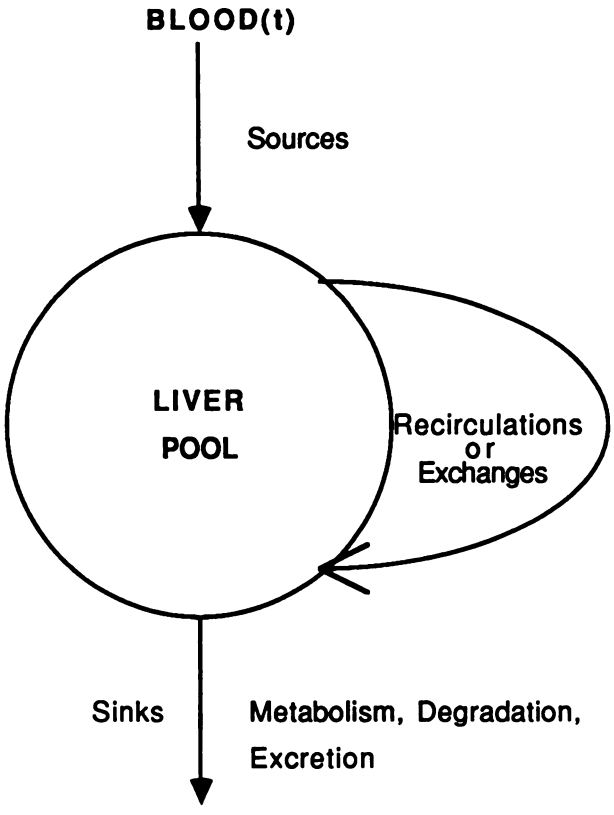

FIGURE 2
Noncompartmental model for HIDA kinetics. The liver pool is the central pool into which is input tracer from the blood. The liver is not modeled explicitly in this case, but any number of recirculations or exchanges can occur. Tracer is assumed to leave the liver pool directly via either metabolism, degradation, or excretion. In the case of HIDA kinetics it leaves via excretion or radioactive decay.

Patients Studied

A total of 20 scans from ten adult patients (with various liver abnormalities) were used for testing model configurations. The preferred model configuration was then applied to 97 scans from 39 pediatric liver-transplant recipients to estimate the model parameters and MRT. A noncompartmental method for estimating MRT^{nc} was also used in these patients. The pediatric scans were not used to test various model configurations because of the typically greater noise in these studies because of patient movement.

Time-Activity Curves

Regions of interest (ROIs) were drawn over the lateral portion of the liver (to minimize radioactivity from the gastrointestinal (GI) tract and kidneys) and the heart, producing, respectively, the observed liver time-activity curve ($L_0(t)$) and the heart (blood pool) time-activity curve (B(t)). The counts in each ROI were normalized by scan length to obtain cts/pixel/min for a given ROI. The time-activity curves were subsequently decay corrected.

The heart blood time-activity curve has been shown to agree well with directly measured blood concentrations of [^{99m}Tc]HIDA compounds in animals (*18*), and was therefore used as an approximation to the true blood time-activity curve. The observed liver time-activity curve represents several components. The liver ROI data consists not only of the activity in the hepatocytes, but also in the intrahepatic bile. Also, some fraction (f) of the blood pool is superimposed on the true liver time-activity curve (L(t)), to give the observed liver time-activity curve [$L_0(t) = L(t) + fB(t)$]. This fraction will depend on the relative blood volume of the liver and extrahepatic blood superimposed on the liver ROI.

Compartmental Models

Two categories of compartmental models were tested; one assuming a delta function input into the blood compartment and a second using the observed blood-pool time-activity data B(t) as an input function into the liver compartment(s). The first category models the blood compartment directly and therefore fits both the observed heart blood time-activity curve and the liver time-activity curve simultaneously while using a delta function (approximated by a triangular input of height h_0, and width 0.001 sec) as the input into the blood compartment to simulate the bolus injection of tracer. The height h_0 becomes a parameter to be estimated for each model of this type.

The second type of model tested uses the response in the blood compartment as an input into the liver compartment(s), thus only fitting the liver time-activity curve. An example of this type of model is shown in Figure 3. The blood compartment is not explicitly shown. The liver is represented by two compartments: liver parenchyma and intrahepatic bileducts. The box around these compartments represents that the observed activity to be fitted to this type of model is a combination of activity from both the liver parenchyma and intrahepatic bile. Tracer is taken up by the liver from the blood as represented by k_{21}, it can back-exchange to the blood pool as given by k_{12}. There is unidirectional transfer from the liver

parenchyma to the intrahepatic bile (k_{32}), and a unidirectional exchange from the intrahepatic bile compartment to out of the liver (k_3). A constrained version of this model with $k_{32}=k_3$ was also tested. This constraint implies that the steady state distribution volumes of the tracer in the liver parenchyma and intrahepatic bileducts are equal. In order to test the limitations of assuming this constraint, some of the adult studies were fitted by assuming $k_{32}=c^*k_3$, with c ranging between one-third and 3. A model where the liver is represented by one compartment only was also tested. Each model tested was described by standard state equations as used in system theory (*19, 20*):

$$\dot{x}(t) = [A]x(t) + [B]u(t) \quad (1)$$

$$y(t) = [C]x(t). \quad (2)$$

Here, x(t) is a vector with components representing the activity in each compartment of a particular model, $\dot{x}(t)$ is a vector with components representing the time rate of change of activity in each compartment, u(t) is a vector with components representing the input into each compartment, and y(t) is a scalar representing the total observed activity. The matrices [*A*], [*B*], and [*C*] are functions of the model parameters. As an example, these equations for the model of Figure 3 (with $k_{32}=k_3$) are given by:

$$[A] = \begin{bmatrix} -(k_3 + k_{12}) & 0 \\ k_3 & -k_3 \end{bmatrix} [B] = \begin{bmatrix} k_{21} \\ 0 \end{bmatrix}$$
$$[C] = [1, 1] \quad (3)$$

Every model studied was used in conjunction with the 20 adult scans to fit for the model parameters directly via nonlinear regression. This process was facilitated with a software package BLD (*21*). Incorporated into the curve fitting was the parameter f (fraction of blood pool observed in the measured liver time-activity curve) by changing Equation (2) above to y (t) = [C] x(t) + fB(t). For each model, fitting was also performed by fixing f=0. Also, because the counts observed are actually the integrated activity over the scan duration, the time integral of activity was directly accounted for in the state Equations (1 and 2), and the fits repeated for some of the adult scans (*20*). The parameter correlation matrix was obtained for the best fitting model when fit to some of the scans in order to provide insight into how the parameters of the model are related. The MRT was calculated from the expected observation y(t) for a unit impulse for a particular model configuration and Equation (4).

$$MRT = \frac{\int_0^\infty y(t)\,dt}{y(0)}. \quad (4)$$

As an example, the MRT for the model of Figure 3 (with $k_{32}=k_3$) is obtained by solving for y(t) from Equations (1), (2), and (3) giving:

$$y(t) = x_2(t) + x_3(t)$$
$$= (k_{21} - k_{21}k_3/k_{12})e^{-(k_{12}+k_3)t} + (k_{21}k_3/k_{12})e^{-k_3t}, \quad (5)$$

where $x_2(t)$, $x_3(t)$ represent the activities in the liver parenchyma and intrahepatic bileducts compartments respectively. The substitution of Equation (5) into Equation (4) yields MRT = $2/(k_{12} + k_3)$ for the model of Figure 3 (with $k_{32} = k_3$).

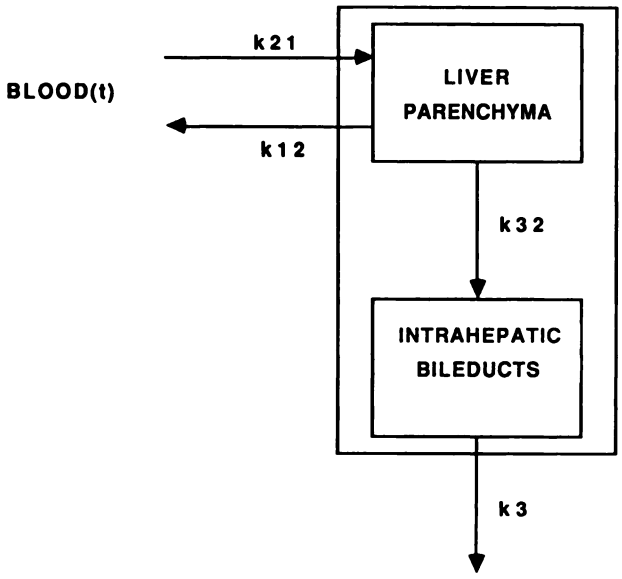

FIGURE 3
A three-compartment tracer kinetic model in which the blood compartment is not modeled directly, but instead the activity in blood is used as an input function into the liver parenchyma compartment. The liver is modeled as the liver parenchyma compartment and intrahepatic bileducts compartment. The box around these two compartments represents that the observed activity in the liver is a combination of activity from both these compartments. k_{21} governs tracer uptake by the liver from the blood. k_{12} governs tracer back-exchange from liver to blood. k_{32} governs exchange of tracer between the parenchyma and intrahepatic bile ducts, and k_3 the exchange out of the intrahepatic bile ducts.

Noncompartmental Analysis

The time-activity curves were also fitted for using a noncompartmental technique based on parametric deconvolution. Let $L_0(t)$ be the observed liver time-activity curve, let B(t) be the observed heart blood time-activity curve. Let $L_\delta(t)$ be the response of the liver to a delta input, then $B(t) \otimes L_\delta(t) = L_0(t)$, where $\otimes$ represents the convolution operator. This equation was mathematically deconvolved to fit for parameters p_1–p_4 by assuming that $L_\delta(t) = p_1e^{-p_2t} + p_3e^{-p_4t}$ ($p_i > 0$ {i=1:4}). The noncompartmental mean residence time MRT^{nc} was then calculated using:

$$MRT^{nc} = \frac{\int_0^\infty L_\delta(t)\,dt}{L_\delta(0)} = \frac{\frac{p_1}{p_2} + \frac{p_3}{p_4}}{(p_1 + p_3)} \quad (6)$$

Acquisition Length and Scanning Frequency

The effect of acquisition length on the estimates of the model parameters was tested by fitting the parameters of the best fitting model over a range of acquisition times for some of the adult studies. This was done by truncating the time-activity data and refitting for the model parameters. To assess the possibility of using a different scanning protocol, various scanning frequencies were used in conjunction with simulated data from the best fitting model. Using a decaying monoexponential (rate constant = 0.1 min^{-1}) blood time-activity curve and the best fitting model with fixed values of the model

parameters, a liver time-activity curve was generated. Gaussian noise was then added to both time-activity curves. Several scanning frequencies (4 scans/min, 2 scans/min, 1 scan/min, 1 scan/2 min, 1 scan/3 min, 1 scan/4 min) were subsequently used to generate simulated sampling of the blood and liver time-activity curves. These curves were then used in conjunction with the best fitting model to estimate the model parameters. This procedure was repeated over a range of values for the model parameters.

Bilirubin Levels

In order to study the possible effects of total plasma bilirubin levels on the mean residence time and rate constants of the models, total bilirubin levels were obtained (when available) within 12-24 hr of each scan for each patient.

Simulations

In order to assess various features of the compartmental and noncompartmental approach, several computer simulations were performed. Simulated liver time-activity curves corresponding to states of low extraction and low excretion of DISIDA were generated using the best fitting model and a typical heart blood time-activity curve from a patient study.

Because the noncompartmental analysis does not directly account for f, the effects of f on the estimation of MRT^{nc}, was studied with computer simulations. Liver time-activity curves were generated using the best fitting compartmental model for various values of the rate constants and f (while using as an input function the heart blood time-activity curve from an adult study), and then these time-activity curves were analyzed using the parametric deconvolution technique to calculate MRT^{nc}. These estimates of MRT^{nc} were compared to estimates of MRT calculated directly from the pre-defined model parameters (the rate constants).

RESULTS

Model Fitting

Results of the model fitting showed that only the model illustrated in Figure 3 with $k_{32}=k_3$ was able to converge for all the 20 sets of time-activity curves used. No model converged (for all scans) with f fixed to zero. Figure 4 is an example of time-activity curves from two DISIDA studies for a 50-yr-old female who received a liver transplant for primary biliary cirrhosis. The first study was performed immediately after the transplant, and the second study was done when the patient was readmitted (25 days after transplantation) due to increased icterus. Shown in the graphs is the heart time-activity curve, the observed liver time-activity data points, the fitted (by model of Figure 3 with $k_{32}=k_3$) liver time-activity curve going through these data points, and the true liver time-activity curve as determined by subtracting a fraction f (estimated as a model parameter) of the blood curve from the fitted liver curve. Note that the blood-pool activity drops rapidly as a function of time (representing extraction of DISIDA from the blood by the liver and excretion via the kidneys), and the liver activity increases (again representing uptake) and then declines (representing excretion of DISIDA out of the liver) as a function of time. Also listed are the parameter values for k_{21}, k_{12}, k_3, f and their corresponding standard errors. Note the uptake rate constant k_{21} drops over the course of the two studies from 0.77 to 0.47 min^{-1} and the excretion rate constant k_3 also drops over the course of the two studies from 0.09 to 0.002 min^{-1}. Analysis of liver function tests revealed a total bilirubin of 5.8 mg/dl, SGOT=34 U/l, SGPT=89 U/l prior to the second DISIDA study, and a total bilirubin of 1.4 mg/dl, SGOT=9 U/l, SGPT=63 U/l prior to the first DISIDA study. The increase in liver enzymes occurred in conjunction with a decrease in estimates of the uptake rate constant and the excretion rate constant. The patient was assessed to have chronic rejection of the liver, and was given steroid pulse therapy. She responded well with her liver enzymes returning to normal levels.

Results from all 97 pediatric scans had the following means ± s.d. for the parameters estimated: $k_{21}=0.64\pm 0.52$, $k_{12}=0.12\pm0.22$, $k_3=0.10\pm.11$, $f=0.35\pm30$. The

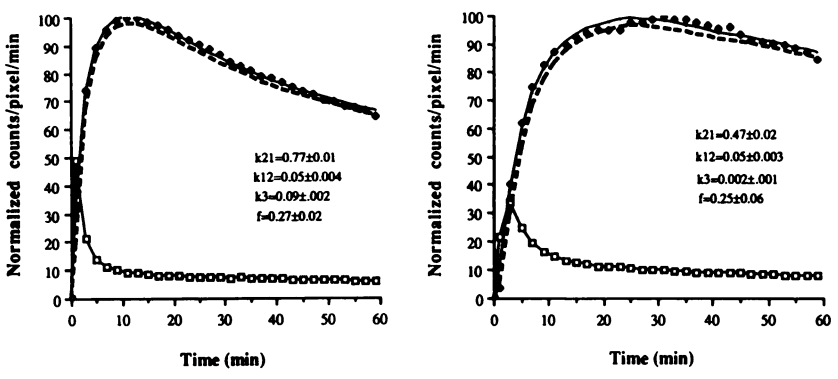

FIGURE 4
Plots of the normalized (relative to maximum counts/pixel/min) liver time-activity data points (solid diamonds), the fitted curve through these points (solid line), and the true liver curve (dotted line) with effects of f accounted for. Also shown is the heart blood time-activity curve (open squares). The two plots are for the same adult over a period of ~ 25 days. Values of the estimated rate constants and f along with their standard errors as obtained by fitting the data to the model of Figure 3 (with $k_{32}=k_3$) are also shown. Note that over the course of the two studies tracer uptake (k_{21}) declines, and tracer excretion (k_3) also declines.

corresponding means of the standard errors of each estimate were: 0.09, 0.05, 0.02, and 0.11.

Results from using the time integrals of activity for each scan duration showed no significant difference ($p<0.05$) in estimates of each of the parameters of the best fitting model (k_{21}, k_{12}, k_3, f) as compared to using the midpoint of the interval for the placement of the activity. This result is expected given that the activity change during a scan interval is relatively slow, and thus a midpoint approximation is good.

The results of a typical correlation matrix for data fitted to the model of Figure 3 (with k32=k3) are

$$\begin{bmatrix} 1 & 0.92 & -0.75 & -0.59 \\ 0.92 & 1 & -0.94 & -0.43 \\ -0.75 & -0.94 & 1 & 0.32 \\ -0.59 & -0.43 & 0.32 & 1 \end{bmatrix}$$

Here the components of the matrix p_{ij} are the correlation coefficients for parameter i and j, where parameter 1 is k_{21}, 2 is k_{12}, 3 is k_3 and 4 is f. The correlation matrix reflects the degree to which errors in the parameter estimates are related. It is seen that k_{12} is highly negatively correlated to k_3 (−0.94), thus if one of these parameters is overestimated the other will tend to be underestimated, and therefore a parameter which takes both of these into account simultaneously (such as the mean residence time $MRT=2/(k_{12} + k_3)$), may be a better estimated quantity which can be followed in a set of patient studies.

Acquisition Length and Scanning Frequency

Figure 5 illustrates the effects of shortening the total scan length on the parameter estimates from a typical adult study. It is seen that all parameters of the model may be estimated well, even for durations as short as 20 min, thus in the future a shorter protocol may possibly be used. Although not explicitly shown, the standard errors of the parameters were found to be higher for shorter scan lengths, while the mean values of the parameters were estimated well. Results from the scanning frequency simulations showed that sampling of at least once every 2 min was necessary in order to give accurate estimates of the model parameters. The greatest effect of sampling frequency is on the model parameters k_{21} and f, both of which are overestimated if the scanning frequency is less than once every 2 min.

Pediatric Scans and Mean Residence Time

A typical heart blood time-activity curve and liver time-activity data as derived from a pediatric scan are shown in Figure 6. Also shown is the fitted liver time-activity curve (using model of Fig. 3 with $k_{32}=k_3$). Notice the greater noise (primarily due to patient movement) in this representative scan, and the ability of the model to converge to a fit nevertheless. The fitted curve is typically noisy because the heart blood time-activity curve is used as an input function. Results of analyzing the 97 pediatric liver transplant scans by both the compartmental model of Figure 3 (with $k_{32}=k_3$) and by parametric deconvolution to obtain, respectively, MRT and MRT^{nc} are shown in Figure 7. Note that in general $MRT^{nc} < MRT$ (r=0.80).

Bilirubin Levels

Shown in Figure 8 is a plot of MRT versus total bilirubin (r=0.13). A statistical test for the slope=0, is not rejected at a significance level $\alpha=0.05$. Shown in Figure 9 is a plot of k_{21} (the uptake rate constant) versus total bilirubin (r=−0.40). A statistical test for the slope=0 is rejected ($p < 0.0001$). If the same test is repeated for data truncated for total bilirubin levels ranging from 0-10 mg/100 ml, a statistical test for the slope=0 is still rejected($p < 0.001$), although the p value is much higher. These graphs indicate that there is a significant effect of bilirubin on DISIDA extraction (although this effect diminishes for lower levels of bilirubin) but not a significant effect on MRT of DISIDA.

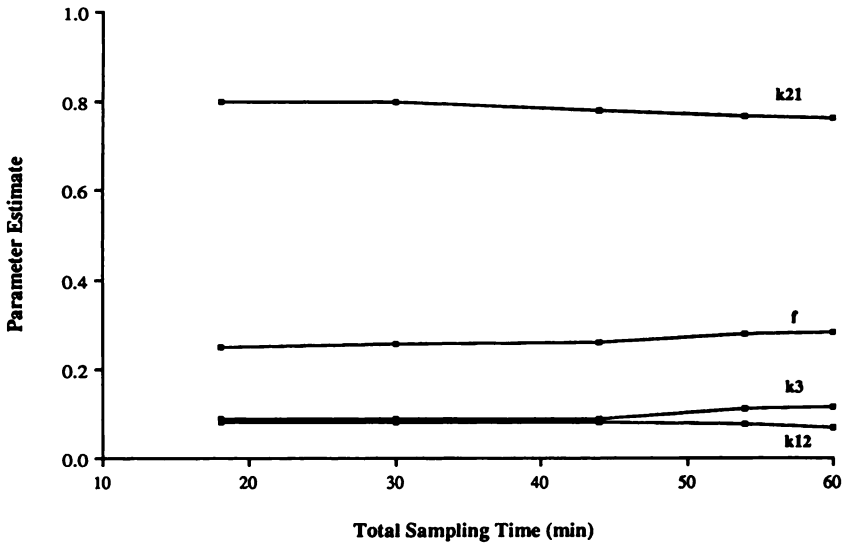

FIGURE 5
A plot of the effects of total sampling time on the estimates of the model parameters as obtained from a typical adult study. Note the flat response over the time interval 20-60 min, thus indicating that shorter acquisition times may be used with minimal change in the mean of the parameter estimates.

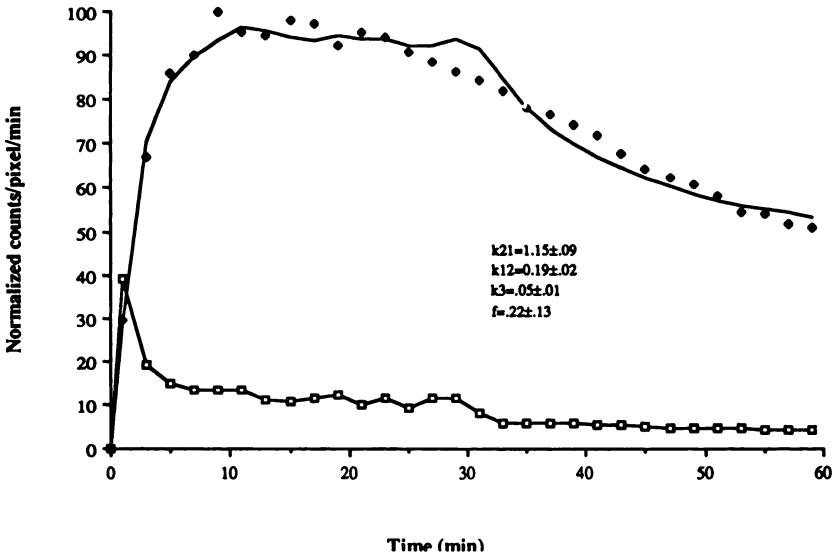

FIGURE 6
A plot of the liver time-activity data (solid diamonds), the fit (using model 3 with $k_{32}=k_3$) through these points (solid line) and heart blood (open squares) time-activity curves in a pediatric scan. The cts/pixel/min are normalized to the maximum counts/pixel/min observed for the scan. Estimates of the model parameters along with their standard errors are also shown. Note the noisy fit to the liver time-activity data points, because the input function (the heart blood–time-activity curve) used is itself noisy.

Distribution Volume Assumption

For some of the adult studies in which the model of Figure 3 was fitted while assuming $k_{32}=c^*k_3$ ($\frac{1}{3} \leq c \leq 3$) it was found that estimates of k_{21} differed (from values obtained for $k_{32}=k_3$) by a maximum of ±8%, and estimates of MRT differed by a maximum of ±15%. The percent difference grows as c deviates from one in either direction.

Simulations

Figure 10 shows the results of simulations to assess how the parameters of the model have an effect on the observed liver time-activity curves. As seen in Figure 10A, by increasing k_{21} (extraction), the relative separation between the heart and liver time-activity curves increases. Increasing k_{12} has a similar effect. Figure 10B shows the effects of increasing k_3. The relative magnitude between the liver and blood time-activity curves decreases with increasing liver excretion, with little change in slope of the liver time-activity curve at later times. Figure 10C shows the effects of increasing f on the observed liver-time activity curve. Not much of a change is seen, except that the peak of the liver time-activity curve shifts closer to the y (counts) axis. These simulation results can be used to aid in subjectively interpreting time-activity curves obtained from a DISIDA scan, without doing any curve fitting.

Results from simulations in which the liver time-activity curve is generated by the model of Figure 3 (with $k_{32}=k_3$) and then deconvolution is used to calculate MRT^{nc}, show that the parameter f can affect the results significantly. Shown in Figure 11 is the percent underestimation of the true mean residence time as calculated by MRT^{nc} as a function of f. For f=0 there is no underestimation ($MRT=MRT^{nc}$) as expected (because the compartmental configuration of Fig. 3 (with $k_{32}=k_3$) is equivalent to a noncompartmental model configuration of Fig. 2), but for f>0 significant under-

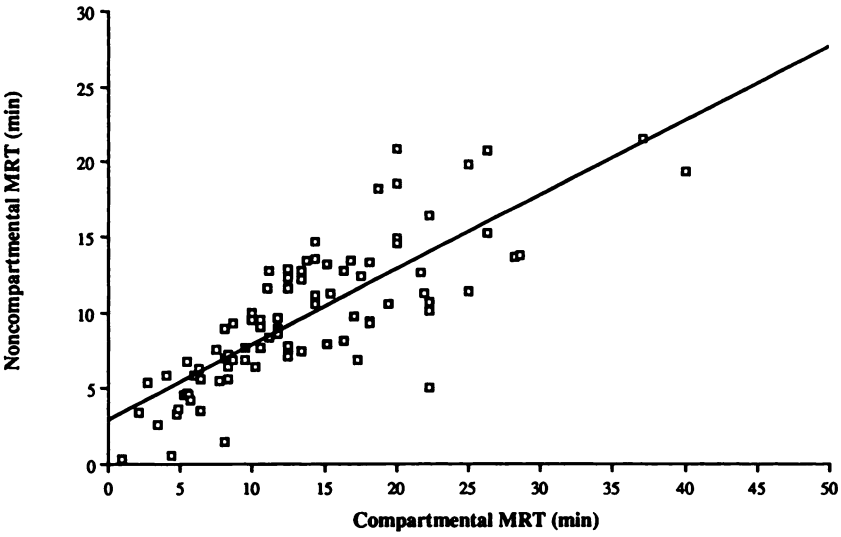

FIGURE 7
Plot of the MRT^{nc} (min) vs. the MRT (min) for the pediatric scans. A linear regression through these points gives a correlation of r=0.80. In general the MRT^{nc} underestimates MRT.

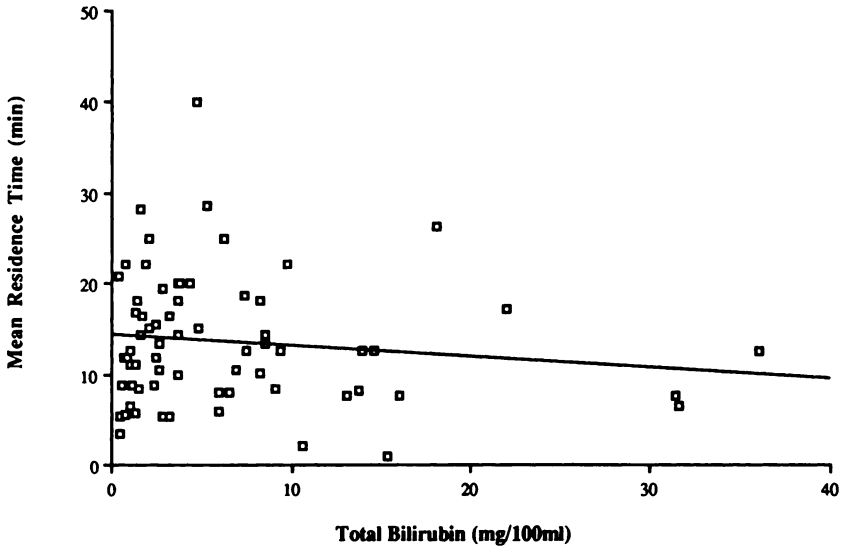

FIGURE 8
Plot of the mean residence time versus total plasma bilirubin levels. The correlation is low (r=0.13). A statistical test for the slope=0 is not rejected at a significance level of α=0.05.

estimation can occur if the MRT is calculated by the deconvolution method. This underestimation is consistently the same for various values of the rate constants (k_{21}, k_{12}, k_3) of model 3 (with $k_{32}=k_3$) used to generate the time-activity curve.

DISCUSSION

The key feature that distinguishes the tracer kinetic modeling approach as applied to scintigraphic studies is that both estimates of the blood time-activity curve (when a suitable blood pool structure such as the heart is within the field of view) and the liver time-activity curve are available for use in model fitting. This allows one to explore various model configurations, as was done in this study, while still maintaining identifiability of the parameters of the model (the rate constants and f, and when used the delta function height h_0). This scintigraphic technique is very convenient because the input function can be derived from image data as opposed to direct blood sampling, but at the expense of absolute quantitation. However, because of intrinsic inaccuracies of the gamma camera technique itself (lack of quantitatively precise attenuation correction, and limited spatial resolution), absolute quantitation is not possible. Additionally, regions of interest on a nontomographic image as used here include activity outside (anterior or posterior to) the organ or area of interest. The observed liver time-activity curve also consists of some fraction f of the heart time-activity curve, both from overlying tissues and because of the activity within the intravascular space of the liver. The results of this study show that a three-compartment model may be used to fit time-activity curves obtained from DISIDA scintigraphy. To choose the model that best supports

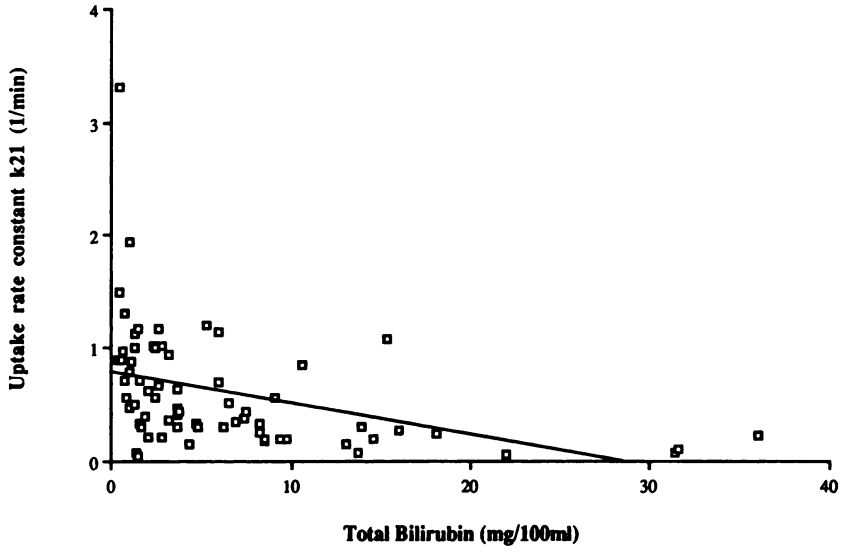

FIGURE 9
Plot of tracer uptake (k_{21}) vs. total plasma bilirubin levels. The correlation is r=0.40. A statistical test for the slope=0 is rejected ($p < 0.0001$).

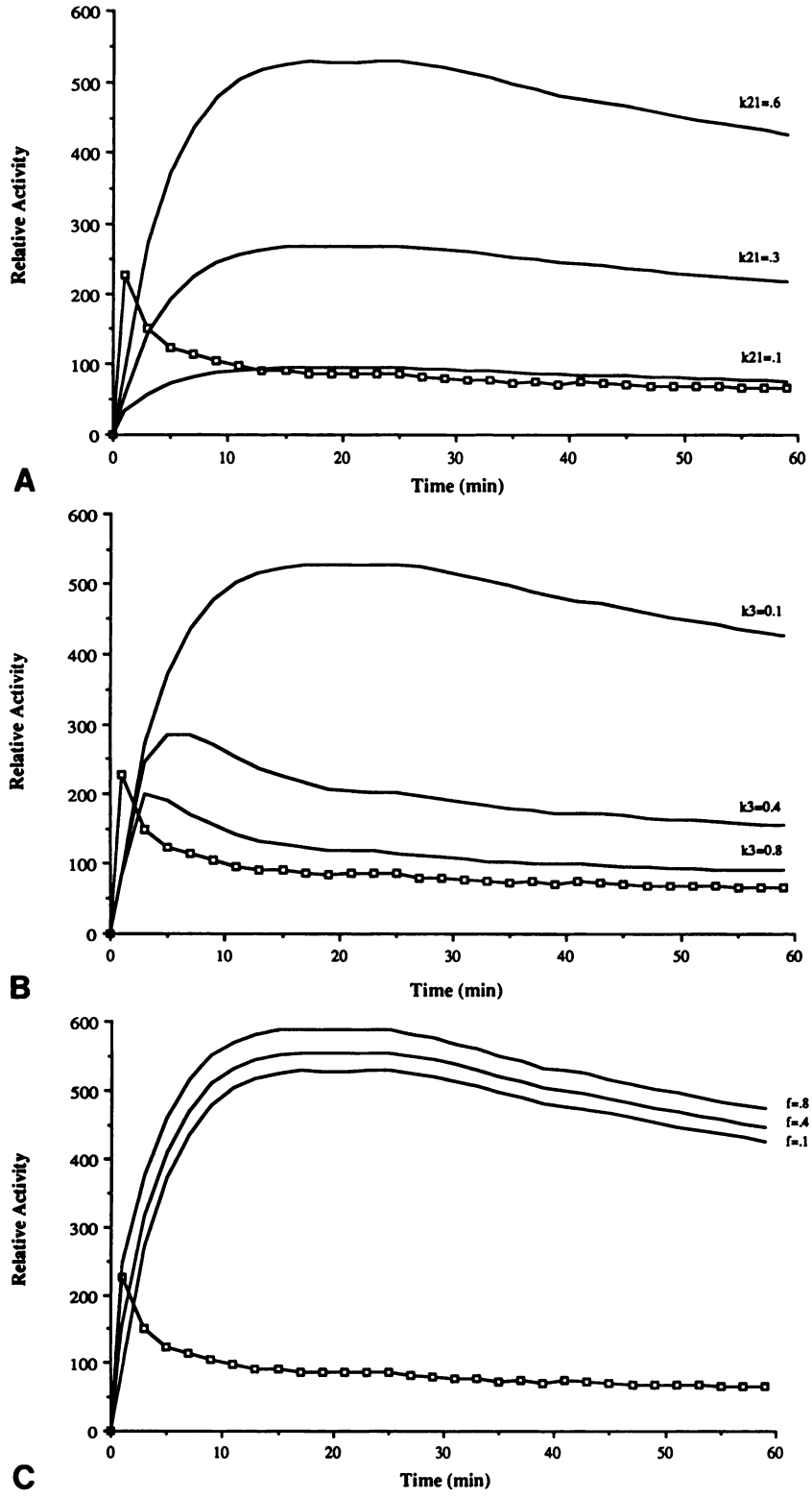

FIGURE 10
A: Plot of the effects of increasing tracer uptake (k_{21}) on the observed liver time-activity curves. Also shown is the input function (open squares) used in this simulation. Note that as k_{21} gets larger, the initial portion of the liver time-activity curve rises faster, and the relative separation between the input function and the liver time-activity curve increases. The other model parameters were fixed at k_{12}=0.1, k_3=0.1, f=0.1. B: Plot of the effects of increasing tracer excretion (k_3) on the observed liver time-activity curves. Also shown is the input function (open squares) used in this simulation. Note that as k_3 gets larger, the relative separation between the input function and the liver time-activity curve decreases. The other model parameters were fixed at k_{21}=0.6, k_{12}=0.1, f=0.1. C: Plot of the effects of increasing f (fraction of blood pool superimposed on the true liver time-activity curve) on the observed liver time-activity curve. Also shown is the input function (open squares) used in this simulation. Note that as f gets larger, the initial rise in the curve increases and the relative separation between the liver time-activity curve and the input function increases slightly.

the data, only the adult studies were used. All but one of the models used were unable to converge over all adult scans, and because the pediatric scans are typically noisier, different model configurations were not tested on these scans. Tracer kinetics of DISIDA are expected to be the same in the two groups of studies, and therefore the best fitting model was used to fit time-activity curves from pediatric scans also. From the fits of this model, estimates of extraction, excretion and mean residence time of tracer in the liver (hepatic parenchyma and intrahepatic bile) may be obtained. This type of modeling approach where the heart blood time-activity

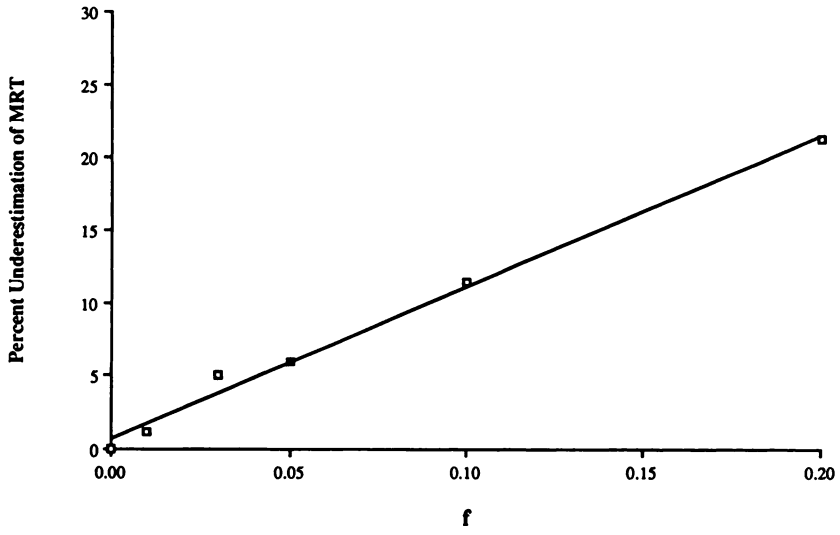

FIGURE 11
The effects of f (fraction of blood pool superimposed on the true liver time-activity curve) on the estimation of the noncompartmental mean residence time. Note that for f=0 there is no underestimation, but as f increases so does the percent underestimation in direct proportion to f.

curve is used as the input function to fit the liver time-activity curve has a distinct modeling advantage. This advantage is that the plasma space does not have to be explicitly modeled, and thus exchanges between the plasma compartment and nonhepatic compartments (ex. the kidneys) do not need to be explicitly accounted for.

There are several assumptions in using the tracer kinetic model of Figure 3 (with $k_{32}=k_3$) to quantitate directional changes in liver function. It is assumed that the heart blood time-activity curve is representative of the blood time-activity curve. While this is an approximation, previous studies in animals have indicated that it is a reasonable assumption (*15*). Furthermore, it is assumed that the heart blood time-activity curve is the input function presented to the liver. This is a simplification, because the liver has a dual blood supply and the input function that is presented to the liver is probably delayed and dispersed as compared to the input function as measured by an ROI drawn over the heart image. It is also assumed that all transport between compartments is first order (the transport rates are products of concentrations and rate constants). The results from this study are consistent with the hypothesis that increasing bilirubin levels are negatively correlated to DISIDA uptake by the liver, although the effect is rather subtle. However, MRT does not seem to be correlated with bilirubin levels, and is therefore perhaps a more useful index of overall liver function. When using the changes in the rate constants to follow a patient, one must correlate the results with measured bilirubin levels, to see if decreases in uptake can in part be explained by changes in bilirubin levels. Since this data was obtained in transplant patients in whom liver function tests, including bilirubin, can be misleading as functional indicators, further clinical testing will be necessary to test this method as a way of mapping directional changes in model parameters.

Implicit to the model of Figure 3 (with $k_{32}=k_3$) is that the distribution volumes of the hepatic parenchyma and intrahepatic bile compartments are equal (because the rate constant leaving the hepatic parenchyma is set equal to the rate constant leaving the intrahepatic bileducts). Although this is probably not the case, one is forced to make a constraint in the parameters, because the data did not support an additional variable parameter in the model fitting. However, it was shown that this constraint is not highly significant because if the constrained value is changed ($k_{32}=c^*k_3$, $\frac{1}{3} \leq c \leq 3$), the effect on parameter estimation (relative to the $k_{32}=k_3$ constraint) was only a maximum percent difference of ±15% for MRT and ±8% for k21. This is not of major significance because it allows for the possibility of the distribution volumes of the two liver compartments differing by as much as three times in either direction, without compromising highly the estimates of the parameters of interest.

Although there are several assumptions underlying the compartmental model, one can nevertheless quantitate directional changes in the model parameters with the use of the scintigraphic time-activity curves. This would allow for the follow-up of liver function in a given patient over a period of time, and may also allow for comparisons among different patients to establish ranges of normal vs. abnormal values. Further work on clinical correlation of model parameters with hepatic function is currently underway.

As this study shows, using the compartmental approach, the fraction f can be estimated along with the rate constants of the model. Accounting for this fraction f is an important factor for accurate quantitation as was shown through the simulation studies. By not accounting for f the mean residence time is underestimated by approximately the value of f itself. Whereas f can be estimated from the kinetic data in the compartmental approach, in most noncompartmental techniques f

can't be directly accounted for and thus MRT^{nc} underestimates the MRT. In the present study f was not accounted for in the parametric deconvolution technique. This was done so as to study the effects of not accounting for f on the calculation of MRT^{nc}, because most noncompartmental techniques [e.g., Fourier deconvolution methods (*12*)] do not make any assumptions about the $L_\delta(t)$ curve, and therefore cannot account for f. It is, however, possible to subtract a preassigned fraction (f_0 of the heart time-activity curve from the observed liver time-activity curve and then perform the deconvolution by various techniques to obtain the estimates of MRT^{nc}. Although it is possible to use the MRT^{nc} in following a given patient, it is not as reliable as MRT because even though the two parameters correlate well, MRT^{nc} changes do not take into account changes in f and thus might not accurately reflect the changes in MRT. This noncompartmental approach can be faster than direct compartmental model fitting of the time-activity curves, but at the expense of underestimation of the mean residence time and no direct estimates of tracer uptake and excretion rates.

CONCLUSION

The three-compartment model (plasma, hepatic parenchyma, intrahepatic bile), used in conjunction with the time-activity curves provides estimates of liver extraction, excretion, and MRT of DISIDA. Estimates of these parameters are inherently limited by the gamma camera technique and assumptions about the blood time-activity curve. However, these estimates, when carefully used with a knowledge of the underlying assumptions of the modeling process and plasma concentrations of total bilirubin, may help to quantitate liver function and correlate it with clinical progress. This study also shows that the mean residence time may also be obtained using noncompartmental methods, but it will underestimate the true value because of the inability of most deconvolution techniques to account for the blood pool fraction (f) superimposed on the true liver time-activity curve. Work is underway to correlate liver function in pediatric liver transplant patients as assessed by laboratory tests and biopsy data with the model estimates of liver function. This work can also be extended to other tracers used in conjunction with scintigraphy, and the quantitation methods presented are easily adapted to nuclear medicine facilities with standard computer resources.

ACKNOWLEDGMENTS

The authors thank Donna Marciano for helping perform the HIDA scans, and Donald Kirkman Mahoney for advice on the manuscript.

REFERENCES

1. Hawkins RA, Hall TR, Gambhir SS, et al. Radionuclide evaluation of liver transplants. *Semin Nucl Med* 1988; 18:199–212.
2. de Jonge MWC, Pauwels EKJ, Hennis PJ, et al. Cholescintigraphy with Tc-99m-diethyl-IDA for the detection of rejection of auxiliary liver transplants in pigs. *Eur J Nucl Med* 1983; 8:485–488.
3. Pors Nielsen S, Trap-Jensen J, Lindenberg J, et al. Hepato-biliary scintigraphy and hepatography with Tc-99m diethy-acetanilido-iminodiacetate in obstructive jaundice. *J Nucl Med* 1978; 19:452–457.
4. Reichelt HG, Popescu HI. The importance of liver uptake and retention indices in assessment of clinical usefulness of hepatobiliary imaging agents. *J Nucl Med* 1979; 20:171–172.
5. Tarolo GL, Picozzi R, Palagi B, et al. Comparative quantitative evaluation of hepatic clearance of diethy-IDA and para-butyl-IDA in jaundiced and nonjaundiced patients. *Eur J Nucl Med* 1981; 6:539–543.
6. Anderson PO, Douglass KH, Mandenhall KG, et al. Deconvolution analysis in radionuclide quantitation of left-to-right cardiac shunts. *J Nucl Med* 1979; 20:502–506.
7. Fleming JS, Goddard BA. A technique for the deconvolution of the renogram. *Phys Med Biol* 1974; 19:546–549.
8. Kennett TJ, Prestwich WV. On the deconvolution of exponential response functions. *Phys Med Biol* 1979; 24:1107–1122.
9. Valentinuzzi ME. Technical note: discrete deconvolution. *Med Biol Eng* 1975; 123–125.
10. Gamel J, Rousseau WF, Katholi CR, et al. Pitfalls in digital computation of the impulse response of vascular beds from indicator-dilution curves. *Circ Res* 1973; 32:516–523.
11. Juni JE, Thrall J, Froelich J, et al.: A simple technique for reducing deconvolution artifact in scintigraphic studies. *Proceedings, Med. Comp. First IEEE Computer Society Int. Conference on Med. Comp. Science/ Computational Medicine.* Vol. 4, 1982: 174.
12. Juni JE, Merion RM, Campbell DA, et al. Diagnosis of liver transplant rejection by scintigraphy with deconvolutional analysis [Abstract]. *J Nucl Med* 1988; 29:790–791.
13. Hernandez M, Rosenthall L. A cross-over study comparing the kinetics of Tc-99m labeled diisopropyl and p-butyl IDA analogues in patients. *Clin Nucl Med* 1980; 5:159–161.
14. Hernandez M, Rosenthall L. A cross-over study comparing the kinetics of Tc-99m labeled diethyl- and diisopropyl-IDA. *Clin Nucl Med* 1980; 5:352–358.
15. Weissmann HS, Freeman LM. The biliary tract. In: Freeman LM, ed. *Freeman and Johnson's Clinical Radionuclide Imaging, Third Edition.* New York: Grune and Stratton, 1980: 879–1049.
16. Chervu LR, Nunn AD, Loberg MD. Radiopharmaceuticals for hepatobiliary imaging. *Semin Nucl Med* 1982; 12:5–17.
17. Distefano JJ, Landaw EM. Multiexponential multicompartmental and noncompartmental modeling. I. Metholodogical limitations and physiological interpretations. *Am J Physiol* 1984; R651–R664.
18. Loberg MD, Nunn AD, Porter DW. Development of hepatobiliary imaging agents. In: Freeman LM, Weissmann MS, eds. *Nuclear Medicine Annual 1981.* New York: Raven, 1981: 1–33.

19. Chen C-T. Introduction to linear system theory. New York: Holt, Rinehart and Winston, 1970.
20. Huang SC, Feng D, Phelps ME. Model Dependency and estimation reliability in measurement of cerebral oxygen utilization rate with oxygen-15 and dynamic positron emission tomography. *J Cereb Blood Flow Metab* 1986; 6:105–119.
21. Carson RE, Huang SC, Phelps ME. BLD: a software system for physiological data handling and model analysis. *Proceedings of the Fifth Annual Symposium on Computer Applications in Medical Care.* 1981: 562–565.